α-emitting mineral inclusions in apatite, their effect on (U-Th)/He ages, and how to reduce it

Pieter Vermeesch[1], Diane Seward[2], Christopher Latkoczy[3]

Martin Wipf[2], Detlef Günther[3] and Heinrich Baur[1]

Abstract

U-Th rich mineral inclusions in apatite are often held responsible for erroneously old (U-Th)/He ages, because they produce "parentless" ^{4}He. Three aspects associated with this problem are discussed here. Firstly, simple dimensional considerations indicate that for small mineral inclusions, the parentless helium problem might not be as serious as generally thought. For example, a mineral inclusion that is 10% the length, width and height of its host apatite needs to be a thousand times more concentrated in U and Th to produce an equal amount of He. Therefore, single isolated inclusions smaller than a few μm are unlikely to contribute significant helium. For larger or more abundant inclusions, the parentless helium problem can be solved by dissolution of the apatite and its inclusions in hot HF. Secondly, besides creating parentless helium, inclusions also complicate α-ejection corrections. Mathematical exploration of this latter problem for spherical geometries reveals that for randomly distributed inclusions, the probability distribution of single-grain ages is predicted to have a sharp mode at the mean age, with tails towards younger and older ages. On the other hand, multiple-grain measurements will yield accurate and precise age estimates if ten or more randomly distributed α-emitting mineral inclusions are present in a sample. Thirdly, thermal modeling indicates that mineral inclusions have a non-trivial but minor ($<5^o$C) effect on the closure temperature. These predictions were tested on apatites from rapidly cooled migmatites of Naxos (Greece) which contain abundant U-rich zircon inclusions. 36 samples were subjected to two kinds of treatment. The "pooled" age (i.e. the synthetic multi-grain age computed from a number of single-grain analyses) of 4 inclusion-free samples (13 apatites), prepared in HNO$_3$ is 10.9 Ma, close to apatite and zircon fission-track ages from the same rock. (U-Th)/He ages of 14 inclusion-bearing samples dissolved in HNO$_3$ range between 9 and 45 Ma, with a pooled age of 22.6 Ma. The ages of 19 HF-treated samples range between 5 and 16 Ma, with 10 of 14 single-grain samples between 9 and 13 Ma and a pooled age of 10.9 Ma. These observations agree with the theoretical predictions and support the addition of HF-treated apatite (U-Th)/He dating to the thermochronological toolbox.

[1]Institute of Isotope Geology and Mineral Resources, ETH-Zürich, Switzerland
[2]Geological Institute, ETH-Zürich, Switzerland
[3]Laboratory of Inorganic Chemistry, ETH-Zürich, Switzerland

1   INTRODUCTION

The (U-Th)/He thermochronometer is based on the α-decay of ^{238}U, ^{235}U, ^{232}Th and the often neglected ^{147}Sm in accessory minerals such as apatite, sphene and zircon. Of these minerals, apatite is by far the most used, because of its relatively well-understood diffusive behavior and uniquely low closure temperature ($\sim 70^o$C; Wolf et al., 1996). The radioactive parent (U and Th) and radiogenic daughter (^{4}He) are measured separately on different types of mass spectrometer, and accurate ages are only possible if all parent and daughter nuclides are accounted for. Fitzgerald et al. (2006) provide an excellent discussion of factors that might violate this requirement, such as α-ejection, mineral and fluid inclusions or He implantation by a U-Th rich matrix. The present paper focuses on arguably the most important complication, which is associated with mineral inclusions rich in U and/or Th. The most common α-emitting mineral inclusions in apatite are monazite and zircon (Farley and Stockli, 2002). Zircon contains up to 5000 ppm U and Th, while Th-concentrations of monazite can be up to 30% (Deer et al, 1992). These inclusions eject He into the surrounding apatite that is measured following degassing by heating with a laser or in a resistance furnace. However, zircon inclusions in particular will not dissolve in the concentrated HNO_3 commonly used to digest apatites prior to U-Th analysis. Hence, a substantial fraction of the measured He may be "parentless".

In the following sections, we will first assess the severity of this problem through some simple order-of-magnitude considerations. As a solution to the "parentless He problem", we propose the dissolution of apatite and inclusions in more aggressive acids, such as hot HF (Carter et al., 2004). However, this does not solve a second complication associated with α-emitting mineral inclusions, namely the way they complicate the α-ejection correction. Typically, α-ejection corrections are made under the assumption of uniform U-Th concentration, but this assumption is clearly violated in the presence of U-Th rich mineral inclusions. A mathematical study of this effect is given in Section 3. Besides complicating the α-ejection correction, inhomogeneous U-Th distributions also have an effect on the diffusive behavior (closure temperature) of the radiogenic helium. Section 4 will illustrate that this is a relatively minor effect. Therefore, the HF-dissolution technique might also be applicable to slowly cooled rocks (e.g., 1 ^{o}C/Ma). However, several studies have reported unresolved problems with slowly cooled rocks, including large data scatter (Fitzgerald, 2006) and (U-Th)/He ages older than fission track ages (Soderlund et al, 2005; Green and Duddy, 2006). To avoid these problems, Section 5 illustrates the effectiveness of the HF-dissolution technique on inclusion-rich apatites from rapidly cooled rocks of Naxos (Greece).

2 PARENTLESS HELIUM AND THE IMPORTANCE OF BEING INCLUSION-FREE

"Erroneous" apatite (U-Th)/He ages have often been attributed to U-Th rich mineral inclusions (e.g., Lippolt et al., 1994; House et al., 1997; Fitzgerald et al., 2006). A very substantial part of many (U-Th)/He studies is spent on selecting inclusion-free apatites under the binocular microscope. Under reflected and transmitted light, with or without polarizers, grains are scrutinized for imperfections and mineral inclusions, in order to avoid the parentless helium problem. But even when no inclusions can be detected with this method, it has been suggested that sub-micron sized inclusions, only visible by electron microscopy or fission-track mapping for uranium inhomogeneity, might produce significant amounts of parentless He (Farley and Stockli, 2002; Ehlers and Farley, 2003).

The validity of these concerns can be assessed by some simple order-of-magnitude calculations. Consider a spherical apatite of radius R^a containing a spherical mineral inclusion with radius R^i. If the inclusion is 10 times smaller than the apatite ($R^i = R^a/10$), then its cross-sectional area is 100 times smaller ($A^i=A^a/100$) and the volume of the inclusion is 1000 times smaller than that of the host apatite ($V^i=V^a/1000$). In other words, an apatite containing (an exceptionally low) 1 ppm U requires such an inclusion to be 1000 times more concentrated in U (i.e. 1000 ppm) for it to produce an equal amount of He (Figure 1). Identical arguments hold for non-spherical geometries. For example, consider a prismatic apatite with 10 ppm of U, containing an inclusion that is 1% of its length, 1% of its width and 1% of its height. Such an inclusion has one millionth the volume of the host grain (Figure 1). It would need to consist of pure uranium to increase the helium by just 10%. Typical apatites used in thermochronology have dimensions on the order of 100 μm, and U-Th concentrations $\sim$10 ppm (Farley, 2002). Zircon inclusions have U and Th concentrations of typically 100-1000 ppm and sometimes up to 5000 ppm, whereas monazite can contain up to 30% of Th (Deer et al., 1992). Therefore, sub-micron sized inclusions may be a less significant source of parentless helium than previously thought, unless they are extremely numerous and their composite volume is more than a ten-thousandth or so of the host apatite. We will now shift our attention away from micro-inclusions and focus on somewhat larger inclusions which do contribute substantial amounts of parentless helium.
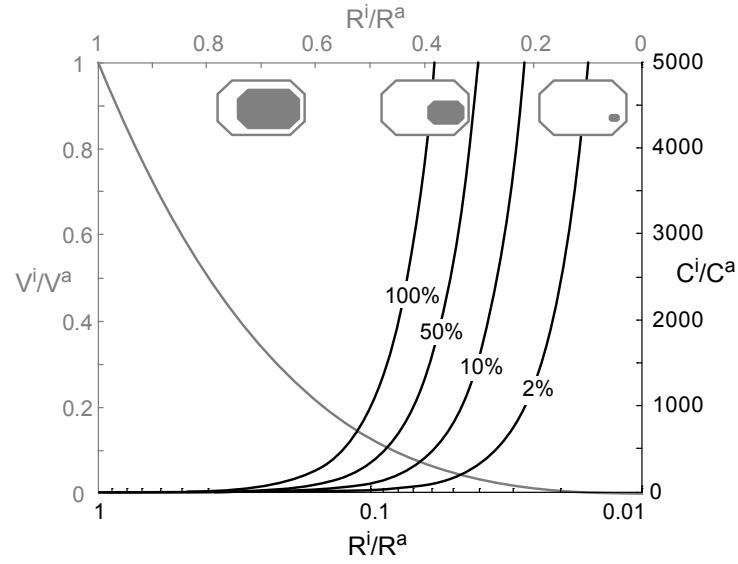
Figure 1: Illustration of the "blessings of dimensionality". The gray line shows, for example, how a tenfold decrease of the linear dimensions of a mineral inclusion (R^i = length, width or height of the inclusion, R^a = length, width or height of the apatite) corresponds to a thousandfold decrease of its volume (V^i for the inclusion, V^a for the apatite) and ^{4}He-production. The black lines show the U or Th concentrations C^i which are required for the inclusion to produce x% of the helium produced by a host apatite with concentration C^a (for x = 2, 10, 50 and 100, respectively). Please note the different horizontal scale for the V^i/V^a and the C^i/C^a curves.

4

3 THE EFFECT OF α-EMITTING MINERAL INCLUSIONS ON α-EJECTION CORRECTIONS

In the previous section, we discussed the magnitude of the parentless helium problem for small mineral inclusions. As will be demonstrated later, it is possible to avoid this problem altogether (even for relatively large inclusions) by dissolving the apatites and their mineral inclusions in aggressive acids such as HF. However, this does not solve a second problem, caused by the inhomogeneous U-Th concentrations associated with mineral inclusions. α-decay of U, Th and their radioactive daughters is associated with energies of 4-8 MeV (Farley et al., 1996). α-particles with such high energies travel on average 20 μm in apatite before coming to rest. Consider a spherical apatite with radius R and an α-emitting nuclide located at a radial distance X from its center. Let S be the α-stopping distance (e.g., 20 μm). α-emitting nuclides located at a distance R-S$\leq$X$\leq$R have a non-zero probability of ejecting an α-particle outside the boundaries of the apatite grain (Figure 2). For any given spatial distribution of U and Th, it is possible to predict the fraction (1-F_t) of radiogenic He lost by α-ejection (Farley et al., 1996; Meesters and Dunai, 2002; Hourigan et al. 2005). In most cases, the U-Th distribution is not known and assumed to be uniform. This assumption often constitutes the bulk of the analytical (U-Th)/He age uncertainty. If significant He is produced by small mineral inclusions, the assumption of uniform composition is violated. We will address this problem mathematically for spherical grain geometries. The physical dimension of the mineral inclusions will be neglected, i.e. they will be considered point sources of α-particles, making the He-retentivity of the inclusion itself irrelevant.

If F_t^a is the α-retention fraction of the apatite, and F_t^i is the fraction of α-particles that are ejected from the inclusion but remain inside the apatite, then the total α-retention factor F_t can be defined as:

$$F_t = GF_t^i + (1 - G)F_t^a \tag{1}$$

where G is the fraction of α-decay activity (π) associated with the mineral inclusion:

$$G = \frac{\pi(inclusion)}{\pi(inclusion) + \pi(apatite)} \tag{2}$$

and $\pi = 8^{238}\lambda[^{238}U] + 7^{235}\lambda[^{235}U] + 6^{232}\lambda[^{232}Th] +^{147}\lambda[^{147}Sm]$ \tag{3}

5

with $^n\lambda$ the decay constant and [n] the number of atoms or moles of nuclide n (for n = 238, 235, 232 or 147). Note that equation 3 considers He-production to be a linear function of time, which is a good approximation for relatively young samples ($t \ll 1/^n\lambda \ \forall$ n). Our goal is to derive the probability distribution of F_t. To achieve this goal, we first compute the cumulative distribution function (cdf) of the α-retention factor F_t^i:

$$cdf_{F_t^i}(f_t^i) \equiv Pr(F_t^i \le f_t^i) = \begin{cases} 0 & \text{if} \quad (2 - S/R)/4 > f_t^i \\ 1 - cdf_{X^*}(x^*) & \text{if} \quad (2 - S/R)/4 \le f_t^i < 1 \\ 1 & \text{if} \quad f_t^i \ge 1 \end{cases} \tag{4}$$

$$\text{with } cdf_{X^*}(x^*) \equiv P(X^* \le x^*) = (x^*)^3 \tag{5}$$

Where X^* is the nondimensional radial distance $X^* = X/R$ corresponding to the α-retention factor F_t^i. $cdf_{F_t^i}$ can be computed because there exists a unique mapping between F_t^i and X^* (Figure 2), derived from equation 1 of Farley et al. (1996):

$$F_t^i(X^*) = \frac{1 - \left(X^* - \frac{S}{R}\right)^2}{4\frac{S}{R}X^*} \tag{6}$$

$$\text{and } X^*\left(F_t^i\right) = \left(\frac{S}{R}\right)\left(1 - 2F_t^i\right) + \sqrt{4\left(\frac{S}{R}\right)^2\left(F_t^i - 1\right)F_t^i + 1} \tag{7}$$

The probability density functions (pdfs) are then easily obtained by taking derivatives of the cdfs:

$$pdf_{F_t^i}(f_t^i) = \frac{d(cdf_{F_t^i}(f_t^i))}{d(f_t^i)} \tag{8}$$

$$\text{and } pdf_{X^*}(x^*) = \frac{d(cdf_{X^*}(x^*))}{d(x^*)} = 3(x^*)^2 \tag{9}$$

Using equations 8 and 9, we can calculate $\bar{F}_t^i$, the expected value of F_t^i assuming that the inclusions have a spatially uniform distribution. Here we use "expected value" in the statistical sense of the word, meaning the average F_t^i of many apatites containing a few inclusions, or the average F_t^i of a few apatites containing many inclusions. Thanks to the mapping between F_t^i and X^* (equations 6 and 7 and Figure 2), $\bar{F}_t^i$ can be calculated either by integrating over F_t^i or over X^*. Not surprisingly, both approaches yield the same result,
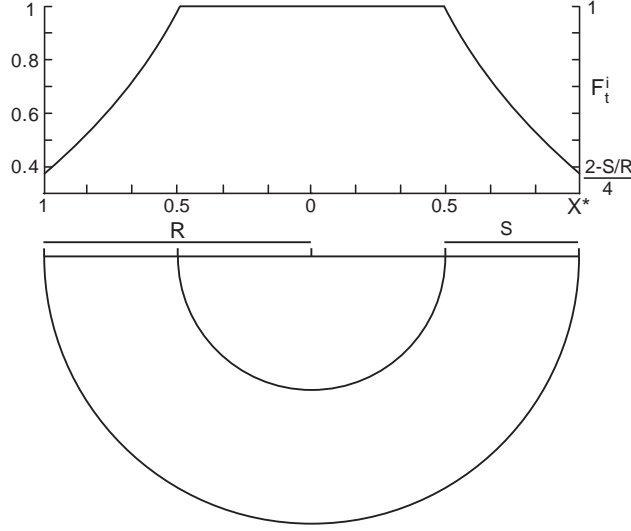
6

Figure 2: Bottom: cross-section through the lower hemisphere of a spherical apatite with radius R. Top: α-retention factor F_t^i for U-Th-bearing mineral inclusions as a function of the non-dimensional radial distance X^*. All ^{4}He produced by inclusions located at $X^* < 1-S/R$ will remain inside the host apatite ($\Rightarrow F_t^i=1$), with S the α-stopping distance. However, inclusions located at $X^* > 1-S/R$ will eject a fraction $(1-F_t^i)$ of helium outside the boundaries of the apatite.

which turns out to be the analytical solution for F_t^a under spherical geometry calculated by Farley et al. (1996) for compositionally homogeneous apatite:

$$\bar{F}_t^i = \int_0^1 f_t^i \; pdf_{F_t}(f_t^i) \; df_t^i = \int_0^1 F_t^i(x^*) \; pdf_{X^*}(x^*) \; dx^* = \dots = 1 - \frac{3}{4}\frac{S}{R} + \frac{1}{16}\left(\frac{S}{R}\right)^3 = F_t^a \qquad (10)$$

The probability distribution of F_t (equation 1) can be calculated for any G from the probability distribution for F_t^i (equation 8) and the expression for F_t^a given by Farley et al. (1996) and equation 10 (Figure 3). Although G is not known in most cases, our ignorance about G can be quantified by assigning a probability density function pdf_G to it. Again, to derive the probability distribution of F_t, we must first define its cumulative density function cdf_{F_t}:

$$cdf_{F_t}(f_t) = \int_0^1 cdf_{F_t^i}\left(\frac{f_t + (g-1)F_t^a}{g}\right) \; pdf_G(g) \; dg \qquad (11)$$

with $cdf_{F_t^i}(\cdot)$ as defined in equation 4, after which pdf_{F_t} is obtained by taking the derivative:

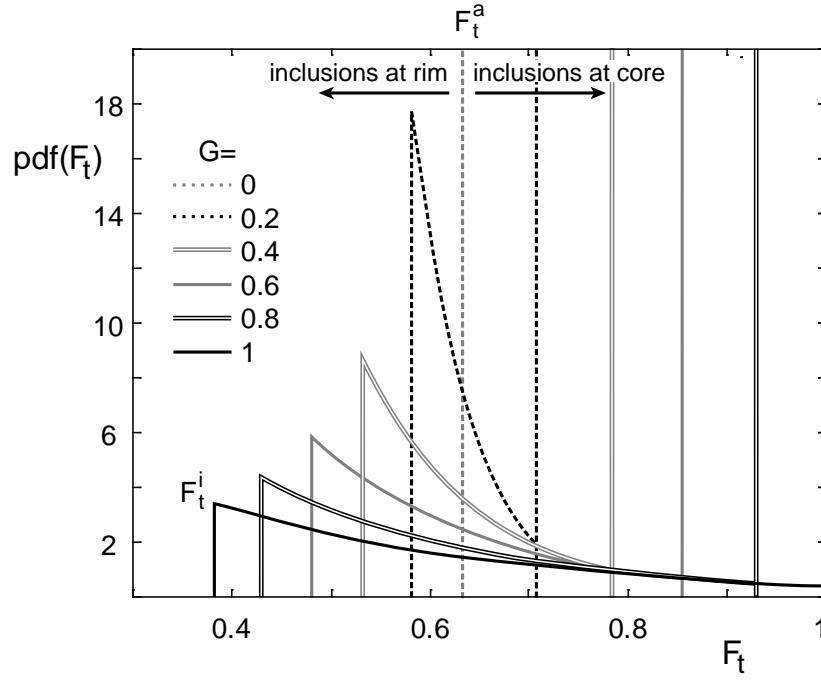$$pdf_{F_t}(f_t) = \frac{d(cdf_{F_t}(f_t))}{d(f_t)} \qquad (12)$$

7

Figure 3: The expected spread of α-retention factors F_t for grains of a single size (S/R = 0.5) if the inclusions are located in different radial positions within a spherical apatite grain. The six curves correspond to inclusions of different α-emitting activity (G-value, equation 2). More helium will be retained from apatites containing an α-emitting mineral inclusion at their core than from inclusion-free apatites or apatites containing an inclusion near their rim.

Figure 4 shows pdf_{F_t} for a uniform pdf_G distribution and various S/R-values. The mode of the distribution is always at F_t^a, with heavy tails, especially toward high α-retentivities. If a "normal" α-ejection correction is made ($F_t \equiv F_t^a$) the most frequently measured age will be accurate, but some other measurements will not. "Undercorrected" ages will generally be further removed from the true age than "overcorrected" ages. It would be relatively easy to compute F_t- and corresponding age-distributions for different, and possibly more realistic pdf_Gs such as the logistic normal distribution. However, such an exercise is of limited interest because in reality, pdf_G is not known. Nevertheless, the main features of Figures 3 and 4 are robust: the mean value of F_t^i equals F_t^a and therefore the mean value of F_t is independent of pdf_G. The distribution of F_t has a sharp mode at F_t^a, with tails towards lower and higher values (Figure 4).
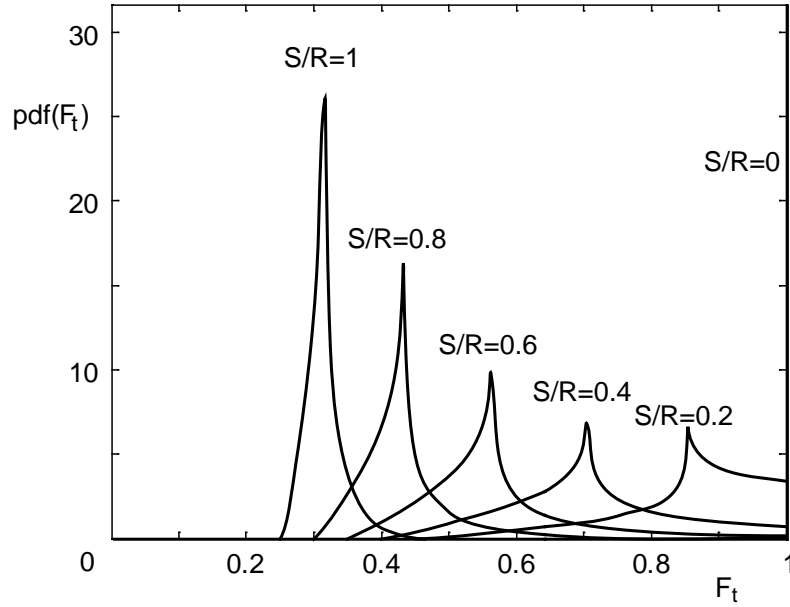

Figure 4: Probability density of the true α-retention factor F_t for uniform G-distribution ($pdf_G(g)\,dg = 1/dg$ for $0 \le g \le 1$) and various grain-sizes (S/R-values). Each of the curves is the result of "stacking" the curves of Figure 3.

Given the probability distribution of F_t (equation 12), the standard deviation of F_t can be calculated as:

$$\sigma(F_t) = \int_0^1 \left(f_t - \bar{F}_t\right)^2 pdf_{F_t}(f_t)\,d(f_t) \tag{13}$$

Where $\bar{F}_t = F_t^a$ (equations 1 and 10). The relative spread ($\sigma(F_t)/F_t$) of the single grain α-retention factor F_t depends on the grain size (Figure 5). For very small grains (S/R > 2), the spread is zero because

all [4]He is ejected ($F_t = 0$), irrespective of the presence or absence of mineral inclusions. For very large grains (S/R $\approx$ 0), the spread of F_t is also zero, because all [4]He stays within the apatite ($F_t \approx 1$) and the chance that a mineral inclusion is located within the outermost fraction S/R of such an apatite is negligible. However, between these two extremes, the spread of the α-retention factors is non-zero, reaching a maximum at S/R $\approx$ 0.6, where $\sigma(F_t)/F_t \approx 0.2$. Please note that because the F_t-distribution is not normally distributed (Figure 5), the 2σ-value of 40% must not be interpreted as the usual 95% confidence interval. However, by virtue of the Central Limit Theorem, the average of n single-grain measurements converges to a normal distribution with standard deviation $\sigma(F_t)/\sqrt{n}$. For example, the expected 2σ-spread (corresponding to a 95% confidence interval) of F_t-values for multi-grain packages containing n=10 grains each with one inclusion, or single grains with n = 10 inclusions is less than 12%. If S/R = 1/3 (e.g., S = 20 μm and R = 60 μm), then the 2σ confidence interval for F_t is $\sim$ 10% (Figure 5). These estimates are conservative because they assume that all the U and Th is contained in the mineral inclusions and that the host apatite itself contains no U or Th. If this is not the case, then the spread of the multi-grain ages will be smaller.
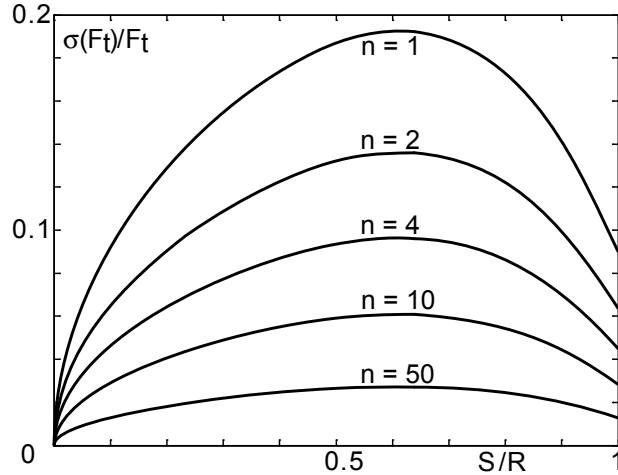

Figure 5: Relative spread of the α-retention factors F_t as a function of grain-size (S/R) and for different multi-grain sample sizes (n = 1, 2, 4, 10 and 50 grains, with $\sigma(F_t|n) = \sigma(F_t|1)/\sqrt{n}$).

4 THE EFFECT OF α-EMITTING MINERAL INCLUSIONS ON CLOSURE TEMPERATURES

Besides complicating the α-ejection correction, the inhomogeneous U-Th-distribution inherent to inclusion-bearing apatites also affects the diffusive behavior of the helium. This problem is well studied in the case of concentrically zoned spherical crystals (Meesters and Dunai, 2002b). The "closure temperature" (defined below) of the (U-Th)/He system depends on the spatial distribution of the helium. This does not constitute a significant problem for relatively rapidly cooled rocks (e.g. > 10 ^{o}C/Ma for rocks older than $\sim$10 Ma). However, for slowly cooled rocks, the effect of mineral inclusions on helium diffusion might induce significant scatter in the apparent ages, depending on the spatial distribution of the inclusions and their relative α-emitting activity (G-factor, equation 2), which are nearly impossible to measure. To get a handle on the significance of this effect, this section will consider the "worst case scenario" of a spherical U-Th-free apatite containing an α-emitting micro-inclusion at its core or rim. Such a grain should have the most different diffusive behavior compared to the default case of an inclusion-free apatite containing a homogeneous U-Th-distribution.

Before proceeding with the analysis, it is useful to recall the definition of "closure temperature" by Dodson (1973). First consider the case of isothermal diffusion for a simple geochronometer defined by one radioactive parent P (e.g., ^{40}K) decaying to a radiogenic daughter D (e.g., ^{40}Ar). At high temperatures, the radiogenic daughter escapes from mineral grains as soon as it is formed whereas at low temperatures, thermally activated diffusion is negligible and the daughter products are quantitatively retained. Now consider the case of monotonic cooling. In the high-temperature part of the cooling-curve, the D/P-ratio stays zero. Under transitional temperatures, the D/P-ratio increases at a rate that increases with time. Finally, at low temperatures, D/P increases linearly with time. The apparent age is the time intercept of the linear section of the D/P vs time curve. This age corresponds to a particular temperature in the cooling history, the so-called "closure temperature" T_c. If the cooling curve is linear in the temperature T, then the closure temperature (T_c) is the temperature intercept of the linear section of the T vs D/P curve (Figure 6). If the cooling curve is linear in 1/T, then T_c can be calculated analytically (Dodson, 1973). Things are a little more complicated for (U-Th)/He because there are not one but three radioactive parents (^{238}U, ^{235}U, and ^{232}Th) with different half-lives, causing their relative contributions to change with time. However, the helium content of young rocks does increase linearly with time to a very good approximation (t $\approx$ [He]/π with π as

defined in equation 3). Therefore, the closure temperature concept can also be used for (U-Th)/He. Because we are interested in the relationship between mineral inclusions and cooling rate (dT/dt), we will assume linear cooling (dT/dt = constant with t). We will not calculate T_c using Dodson's approximate analytical solution (an exact solution is only possible if $T \propto 1/t$). Instead, we will calculate T_c numerically using the DECOMP program of Bikker, Meesters and Dunai (Dunai, 2005).

As said before, in the case of linear cooling T_c is the temperature-intercept of a curve plotting temperature versus apparent (U-Th)/He age (Figure 6). Thanks to a combination of the "superposition principle" (Meesters and Dunai, 2002a & b) and the spherical symmetry, a concentrated α-emitting inclusion is mathematically equivalent to a thin spherical shell at the same distance of the rim (A.G.C.A. Meesters, written communication, July 2006). A spherical shell of a certain U-Th concentration produces as much He as a half-shell with twice, or a quarter-shell with four times this U-Th concentration. By induction it follows that a U-Th rich spherical shell is equivalent to a point source of equal α-emitting activity located at the same distance from the rim. Therefore, individual inclusions can be adequately modeled as spherical shells in DECOMP. The "worst case scenario" of a single α-emitting micro-inclusion located in the center of a U-Th-free apatite was modeled in DECOMP by a spherical zone of 1 μm radius containing all the U and Th, contained in a much larger spherical host apatite (e.g., R = 60 μm in Figure 6), whereas an inclusion located on the rim of such an apatite was modeled by a spherical shell of 1 μm thickness. Given a user-defined cooling curve (10 ^{o}C/Ma for Figure 6), DECOMP forward-models the apparent age through time using an eigenmode-decomposition method (Meesters and Dunai, 2002a & b). In this paper, we used 100 eigenmodes. The apparent age increases linearly with time in the lower temperature part of the linear cooling model (Figure 6). As expected, the linear section of the T-t curve begins at higher temperatures for the apatite containing an inclusion at its core than for inclusion-free apatite. Intuitively, this makes sense because the helium produced by the inclusion must "travel further" before reaching the edge of the apatite. The opposite is true for apatites with an inclusion on their rim.

The closure temperature calculation was repeated for different grain-sizes (40 μm $\leq$ R $\leq$ 130 μm) and cooling rates (10 ^{o}C/Ma and 1 ^{o}C/Ma) (Figure 7). In the "worst case scenario" of an inclusion-bearing apatite, T_c is 5-10 ^{o}C higher or lower than in the absence of inclusions. This is a small effect in several respects. First of all, the "worst case scenario" used for the calculations of Figure 7 is very unlikely to ever occur in nature. As explained in Section 2, mineral inclusions never contain 100% of α-emitting activity,

because their relative volume is small and the U-Th content of apatite is never zero. Consider the more realistic scenario of a mineral inclusion contributing 50% of the total helium (G = 0.5). Because of the superposition principle, such an inclusion will change the closure temperature by only 2.5-5 ^{o}C. The effects of grain size (15-20 ^{o}C difference in T$_c$ between 40 and 130 μm, Figure 7) and cooling rate ($\sim$ 15 ^{o}C difference in T$_c$ between 1 and 10 K/Ma, Figure 7) are greater than the inclusion-effect. Therefore, it should also be possible to apply the HF-dissolution method to slowly cooled rocks. However, several studies have reported irreproducible apatite (U-Th)/He ages for slowly cooled terranes (Fitzgerald et al., 2006) and (U-Th)/He ages older than apatite fission track ages (Soderlund et al., 2005; Green and Duddy, 2006). Therefore, the next section will test the HF-dissolution method on rapidly cooled rocks.
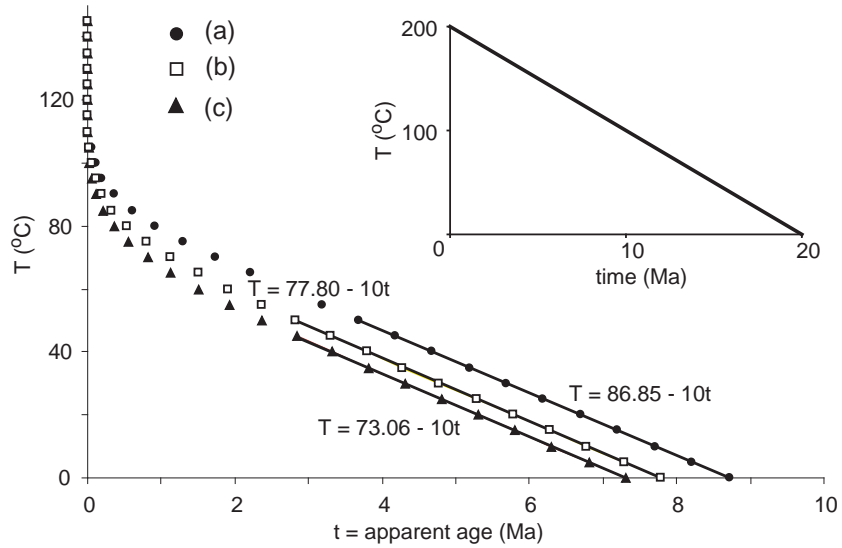

Figure 6: Closure temperature (T$_c$) calculation using the DECOMP program (Dunai, 2005). The inset shows a linear cooling curve with a cooling rate of 10°C/Ma. In this case, the closure temperature can be defined as the y-intercept of the linear section of the temperature vs. age curve (Dodson, 1973). (a) "worst case" scenario of a U-Th-free apatite with a U-Th-bearing inclusion at its center (closure temperature T$_c$ = 86.85 ^{o}C); (b) inclusionless apatite of uniform U, Th concentration (T$_c$ = 77.8 ^{o}C). (c) "worst case" scenario of a U-Th-free apatite with a U-Th-bearing inclusion at its edge (T$_c$ = 73.06). Radius of the host apatite = 60 μm, α-stopping distance S = 20 μm.

13

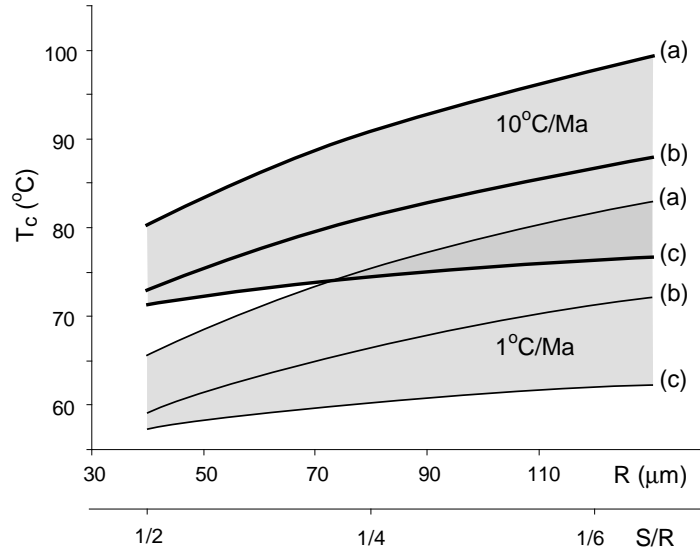Figure 7: Repeating the numerical experiment of Figure 6 for different grain sizes and cooling rates, this plot shows the evolution of closure temperature T_c with grain size, (a & c) with and (b) without the presence of a mineral inclusion in a spherical apatite with radius R, for relatively rapidly cooled (10^oC/Ma, thick lines) and very slowly cooled (1^oC/Ma, thin lines) rocks. (a), (b) and (c) are as defined in Figure 6.

5 APPLICATION TO INCLUSION-RICH APATITES FROM NAXOS, GREECE

From the archive of apatite fission-track samples at ETH-Zürich, we chose a sample that was both rapidly cooled and full of large mineral inclusions. The sample, NAX-3, comes from the migmatite core on the eastern side of Naxos. In fact, apatites from NAX-3 contain so many inclusions that it was quite challenging to date them using the fission-track method. Due to the U bearing inclusions which form "stars" on the mica solid state track recorders (Figure 8), clear grains had to be chosen with care. Nevertheless, a fission-track age of 9.5 ± 1.8 (2σ) was measured using the ζ (zeta) calibration method (Hurford and Green, 1983) (Figure 9.a). The U-concentration of the apatites was determined to be $\sim$20 ppm. Two additional zircon fission-track ages were recorded by Zingg (2004) from the same migmatite at 9.7 ± 1.0 and 10.6 ± 2.0 Ma (2σ) confirming the rapid cooling.
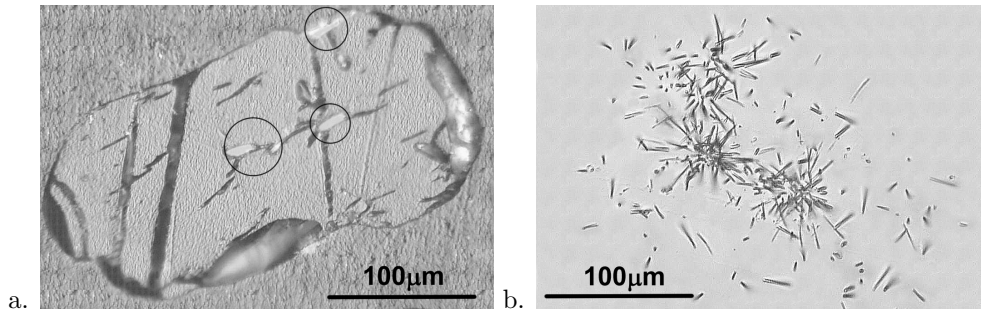

Figure 8: a. NAX-3 apatite with inclusions (encircled) mounted in epoxy; b. The mica-print of the same apatite shows "stars" of induced fission tracks, indicating that the inclusions have a higher U concentration than the surrounding apatite. The inclusions have a smaller effect on the (U-Th)/He age than the track density of the "stars" suggests, because the fission-track map is a two-dimensional cross-section of the apatite, whereas the (U-Th)/He age is based on the three-dimensional, volumetric U-Th-He content of the apatite. To estimate the effect of these inclusions on the (U-Th)/He age, and assuming that the inclusions are 10% of the length of the host apatite, one would effectively have to divide the number of fission tracks in the "stars" by a factor of ten.

Inspection under a binocular microscope (200× magnification) revealed that most inclusions are zircon, based on crystal shape and reflectance (Figure 10). Zircons are the "right" kind of inclusion for the present study, because they are particularly hard to dissolve. After measuring their size under the microscope for the calculation of F_t^a, the apatites were packed in Pt foil tubes. Two batches of grains were prepared: 26 single grain packets and 7 multi-grain packets with inclusion-bearing apatites (labels beginning with "M" in Table 1) and four multi-grain packets with inclusion-free apatites (labels beginning with "Z" in Table 1).
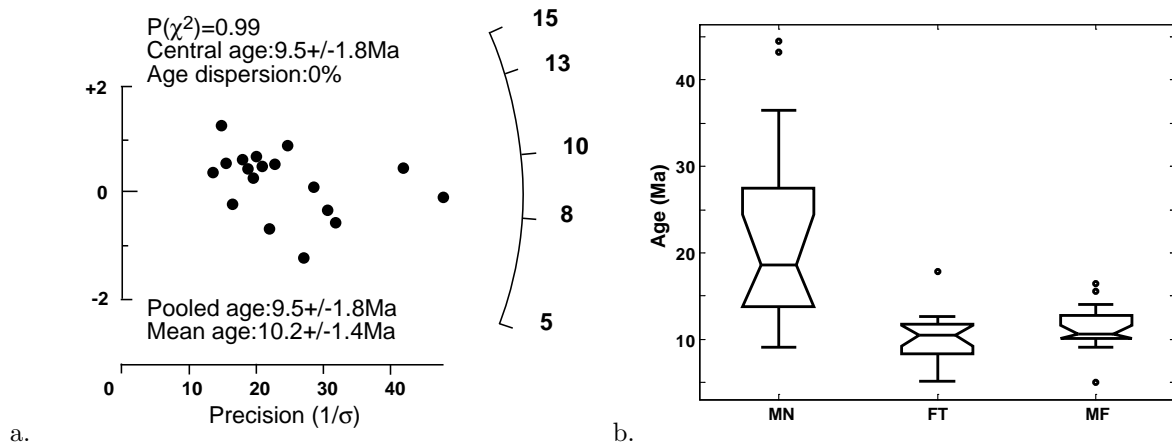
Figure 9: a. Apatite fission-track radial plot (Galbraith, 1990) for NAX-3. b. Box-plots (McGill et al., 1978) for (U-Th)/He data of NAX-3 apatites dated using two acid dissolution treatments: HNO_3 (MN, left side of the figure) and HF (MF, right side of the figure). The middle box plot ("FT") shows the fission track data.

Figure 10: Example of a NAX-3 grain (MF1) with large zircon inclusions. The dimensions of the apatite are $262 \times 127 \times 106$ μm. Pictures a and b show the grain under plain light, whereas picture c was taken under crossed polarizers.

Helium contained in the apatites was extracted during 3 minutes of laser heating under ultra-high vacuum (10^{-8} Torr), using a 1064 nm wavelength Nd-YAG laser. Re-extraction experiments yielded no detectable helium, indicating 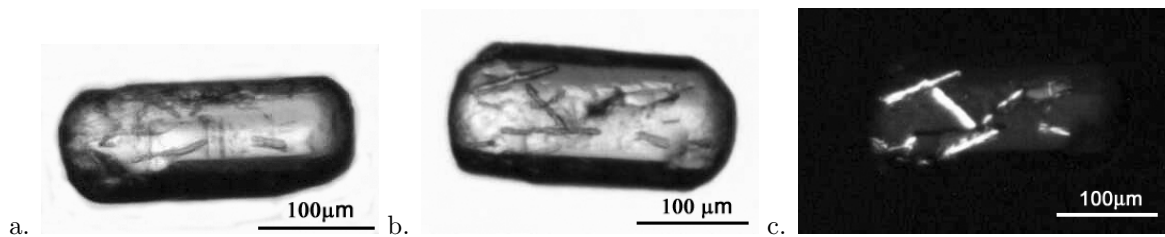complete degassing. Following its release from the samples, the gas was cleaned in a liquid N_2 cooled activated charcoal cold finger and Ti/Zr and Al/Zr getters. ^{4}He was measured by peak height calibration to a bottle of known amounts of ^{4}He in a custom-built sector-type mass spectrometer. After He-analysis, the Pt packets were recovered from the laser pan, partially opened under the binocular microscope, and dropped into teflon bombs. Because Pt dissolves in HF and forms PtAr interferences in the ICP-MS plasma (Reiners, 2005), we had to recover the Pt packets before HF treatment. Using Nb foil envelopes would have been an alternative solution (Reiners, 2005). In nearly half of the cases, dropping the samples into the teflon bombs caused the apatite(s) to fall out of their partially opened packet. These grains were specifically selected for later HF-treatment in order to avoid complications of PtAr interferences. First however, all samples were spiked with $\sim$50 fmol of ^{233}U and $\sim$20 fmol of ^{229}Th. $\sim$1 ml of concentrated and high purity quartz-distilled HNO_3 was added to all the samples. After digestion on a hot plate ($\sim$150°C) for one day, the HNO_3 was dried down for the inclusion-free and half of the inclusion-bearing samples, and $\sim$1 ml of 6%HNO_3-0.8%HF solution was added. For these samples (labels beginning with "MN" and "ZN" in Table 1), this was the final sample preparation step before the U-Th measurement. For the remaining 19 inclusion-bearing samples (labels beginning with "MF" in Table 1), the empty Pt-packets were recovered from the teflon vials prior to evaporation of the concentrated HNO_3. After dry-down, $\sim$1 ml of concentrated, high purity Teflon-distilled HF was added and the samples were bombed in an oven at 200°C for 24 hours and on a hot plate at $\sim$240°C for an additional 48 hours. $\sim$ 100 μl of concentrated HNO_3 was added to the HF for samples MF16-19, following a suggestion of P. Reiners (written communication, May 2006). The HF was dried down and the samples re-bombed in $\sim$1 ml concentrated HCl at $\sim$200°C for 24 hours to dissolve fluoride salts that may have formed during HF evaporation. After a final dry-down, $\sim$1 ml 6%HNO_3-0.8%HF solution was added and the samples were ready for ICP-MS analysis. This combined HNO_3-HF-HCl treatment is tailored to dissolve larger crystals for zircon (U-Th)/He dating (Reiners, 2005). However, zircons inclusions in apatite are generally much smaller, and a less aggressive (e.g., shorter, less hot) procedure might also be suitable.

^{229}Th, ^{232}Th, ^{233}U, ^{238}U (and ^{235}U) were measured in low mass resolution on a single-collector ICP-SF-MS (Element2, Thermo Electron Corporation, Bremen, Germany). The results are summarized in Table 1. Immediate inspection of the data reveals that the spread of the zircon inclusion-bearing grain ages is

much larger for the HNO_3 treated grains than for those treated with HF (Figure 9.b). The former are up to 45 Ma old, whereas the latter cluster more tightly and are closer to the fission-track age. Using the grain dimensions that were measured for the α-ejection correction as an estimate of mass yields median U and Th concentrations of $\sim$5 and $\sim$10ppm for the HNO_3-treated grains, whereas the U and Th concentrations of the HF-treated grains was $\sim$6 and $\sim$14ppm respectively, closer to the fission track estimate ($\sim$19ppm). 10 of the 14 HF-treated single grain samples are between 9 and 13 Ma, consistent with the sharp mode of Figure 4. As discussed in the previous section, the average age of multiple inclusion-bearing apatites should be an accurate estimate of the true age. To compare and combine the single grain measurements with the multi-grain measurements, we introduce a "pooled (U-Th)/He age", which effectively is a weighted mean age obtained by adding the U and Th of several individual analyses, as well as their He-content (weighted for α-ejection), and calculating a synthetic multi-grain age. The pooled age of the HNO_3-treated inclusion-bearing grains is 22.6 Ma, whereas the HF-treated pooled age is 10.9 Ma, which is identical to the pooled (U-Th)/He age of the four inclusion-free apatite analyses. Note that the (U-Th)/He age of one of these four inclusion-free ages is nearly twice as old as the other three. Because we have no indication as to what is the cause of this, we chose not to reject the measurement. However, if the measurement is removed as being unrepresentative the resulting age is 9.2 Ma. Fitzgerald et al. (2006) also observed single grain ages that were several times older than "normal". Perhaps one of the factors discussed by these authors is responsible for this, or a yet unknown complication is at work. As discussed in Section 3 and shown in Figure 5, the spread of HF-treated multi-grain samples should be less than that of the single grain ages. The relative 2σ-spread of multi-grain packages each containing ten inclusion-bearing grains of 100 μm width (equivalent to S/R $\sim$ 0.2) should be less than $\sim$ 8 % (Figure 5). This is confirmed by the five multi-grain measurements of Table 1 (MF15-19), which have a 2σ-spread of just 5%.

sample	# grains	Th [fmol]	2σ	U [fmol]	2σ	He [fmol]	2σ	F_t^a	age [Ma]	2σ
MN1	1	104	4	81	2	3.96	0.14	0.66	44.5	9.3
MN2	1	550	19	2041	50	22.87	0.35	0.85	9.6	0.7
MN3	1	201	7	493	12	11.07	0.21	0.79	20.1	2.2
MN4	1	173	6	283	7	3.89	0.15	0.75	12.5	1.8
MN5	1	119	3	117	3	5.51	0.15	0.68	43.2	8.1
MN6	1	172	7	428	14	8.74	0.17	0.75	19.5	2.7
MN7	1	185	7	371	7	5.90	0.16	0.74	15.1	2.2
MN8	1	160	8	89	3	0.84	0.12	0.58	9.0	2.9
MN9	1	249	7	588	11	11.51	0.22	0.78	17.8	2.0
MN10	1	365	11	725	19	11.56	0.22	0.81	13.7	1.3
MN11	1	144	5	113	2	1.93	0.13	0.64	16.1	3.8
MN12	1	90	18	285	58	6.17	0.08	0.84	20.6	4.6
MN13	8	660	23	2358	73	93.39	1.38	0.79	36.5	4.0
MN14	10	2169	451	2710	554	91.60	0.28	0.85	27.5	5.3
MN (pooled)	30	5342	452	10682	565	345.32	1.55		22.6	1.1
MF1	1	451	14	588	14	9.57	0.17	0.77	14.0	1.8
MF2	1	628	22	874	15	9.75	0.18	0.74	10.1	1.5
MF3	1	768	25	185	4	1.74	0.13	0.76	5.0	0.7
MF4	1	156	5	294	7	4.27	0.14	0.78	12.9	1.5
MF5	1	260	9	596	15	6.97	0.21	0.80	10.4	1.1
MF6	1	370	14	645	17	6.91	0.18	0.73	10.1	1.5
MF7	1	374	10	867	18	10.64	0.22	0.85	10.2	0.7
MF8	1	163	6	222	5	2.02	0.13	0.65	9.3	2.1
MF9	1	136	4	226	5	2.36	0.13	0.79	9.1	1.1
MF10	1	130	4	131	4	2.00	0.13	0.59	16.4	4.7
MF11	1	204	9	357	14	6.42	0.16	0.79	15.6	1.8
MF12	1	126	5	107	3	1.01	0.12	0.63	9.2	2.4
MF13	1	126	26	688	142	9.01	0.10	0.81	12.1	2.6
MF14	1	278	58	1013	212	11.75	0.10	0.86	10.6	2.3
MF15	10	27525	2179	5140	234	121.41	1.82	0.74	11.1	1.6
MF16	10	2557	523	7454	1525	84.64	0.22	0.85	10.1	2.1
MF17	10	1986	406	5610	1146	76.81	0.21	0.85	12.4	2.6
MF18	10	1327	274	3892	806	54.45	0.30	0.83	13.3	3.0
MF19	11	919	190	2578	533	28.01	0.17	0.79	10.6	2.5
MF (pooled)	64	38487	2303	31467	2166	563.09	1.96		10.9	0.6
ZN1	5	151	7	182	8	4.20	0.14	0.70	21.5	3.9
ZN2	3	164	6	262	8	2.20	0.12	0.69	8.2	1.5
ZN3	1	175	5	515	13	4.93	0.14	0.81	8.5	0.8
ZN4	4	175	6	454	11	4.61	0.15	0.68	10.7	2.0
ZN (pooled)	13	666	12	1414	21	21.99	0.28		10.9	0.2

Table 1: (U-Th)/He data for: MN = grains with inclusions, dissolved in HNO_3; MF = grains with inclusions, dissolved in HF; ZN = grain without inclusions, dissolved in HNO_3. The ^{4}He values for the "pooled ages" have been adjusted for α-ejection of the component grains. Age uncertainty includes an arbitrary 20% uncertainty on (1-F_t^a). The pooled 2σ-uncertainties only incorporate the analytical precision and do not reflect the spread of the component single-grain measurements.

6   DISCUSSION

Simple dimensional considerations indicate that single uranium-rich inclusions less than a few percent of the length, width and height of the host apatite are unlikely to contribute substantial radiogenic helium. For larger inclusions or multiple small inclusions, the parentless helium problem can be partially solved by more aggressive acid dissolution procedures. Under the assumption of uniformly distributed mineral inclusions, the average (U-Th)/He age of many inclusion-rich apatites that have undergone such a treatment is accurate. Please note that the assumption of a random distribution can more easily be verified in the presence of large inclusions (e.g., Figure 10) than for micro-inclusions or a compositionally zoned apatite. Grain-selection is significantly faster and easier without the restriction to inclusion-free grains. For some samples, it is nearly impossible to find inclusion-free grains. Further, by broadening the search to include inclusion-bearing grains, it is much easier to find large, euhedral apatites, requiring relatively small α-ejection corrections. Additionally, the presence of U-Th rich inclusions may be an advantage for dating young rapidly cooled rocks. Multi-grain measurements of inclusion-bearing apatites combine the best of two worlds. They have the high U, Th and He content of zircon, but the diffusive behavior and uniquely low closure temperature of apatite. This is similar to the idea behind the work of Min et al. (2006), who dated volcanic olivine and pyroxene using the He produced by the α-emitting inclusions contained within them. On the other hand, dissolving U-Th rich inclusions also causes some complications, particularly for single-grain dating. The probability distribution of single grain ages has heavy tails.

The revised methodology has applications to all rock-types which have inclusion-bearing apatites. However, in most studies, only a few grains are usually dated and it is often possible to find two or three suitable clear crystals. For detrital source studies however, this is not the case because in such studies many more grains are necessary to characterize the population. The difficulty of finding enough inclusion-free grains that represent a realistic and representative cross section of the populations can only be made by also including some of the inclusion-bearing apatites. Although the precision of single grain (U-Th)/He ages on inclusion-bearing apatites is worse than the precision of inclusion-free apatite (U-Th)/He ages, it is comparable to or better than the precision of detrital apatite fission track ages. Thus we recommend that for detrital studies using apatite analysis the more aggressive dissolution method is used routinely.

References

Carter, T. J., Kohn, B. P., Foster, D. A., and Gleadow, J. W. (2004) How the Harcuvar Mountains metamorphic core complex became cool: Evidence from apatite (U-Th)/He thermochronometry. Geology (32) 985-988.

Deer, W.A., Howie, R.A., and Zussman, J. (1992) An Introduction to the Rock-Forming Minerals, 2nd edition. Longman Scientific and Technical Press, 696 pp.

Dodson, M.H. (1973) Closure temperature in cooling geochronological and petrological systems. Contrib. Mineral. Petrol., (40) 259-274.

Dunai, T. J. (2005), Forward modeling and the interpretation of (U-Th)/He ages. Reviews in Mineralogy and Geochemistry, Vol. 58 (ed. P. W. Reiners and T. A. Ehlers), pp. 259-247.

Ehlers T. A. and Farley K. A. (2003) Apatite (U-Th)/He Thermochronometry: methods and applications to problems in tectonics and surface processes. Earth and Planetary Science Letters 206(1-14).

Farley K. A., Wolf R. A., and Silver L. T. (1996) The effects of long alpha-stopping distances on (U-Th)/He ages. Geochimica et Cosmochimica Acta 60(21), 4223-4229.

Farley K. A. and Stockli D. (2002) (U-Th)/He Dating of Phosphates: Apatite, Monazite, and Xenotime. In Phosphates, Reviews in Mineralogy and Geochemistry, Vol. 15 (ed. M. Kohn, J. Rakovan, and J. M. Hughes), pp. 559-578.

Farley, K.A. (2002) (U-Th)/He dating: Techniques, calibrations, and applications. In Noble Gases in Geochemistry and Cosmochemistry, Reviews in Mineralogy and Geochemistry, Vol. 47 (ed. Porcelli, D.P., Ballentine, C.J., and Wieler, R.), pp. 819-844.

Fitzgerald P. G., Baldwin S. L., Webb L. E., and O'Sullivan P. B. (2006) Interpretation of (U-Th)/He single grain ages from slowly cooled crustal terranes: A case study from the Transantarctic Mountains of southern Victoria Land. Chemical Geology 225, 91-120.

Galbraith R. F. (1990) The radial plot; graphical assessment of spread in ages. Nuclear Tracks and Radiation Measurements 17, 207-214.

Green, P. F. and Duddy, I. R. (2006) Interpretation of apatite (U-Th)/He ages and fission track ages from cratons, Earth. Planet. Sci. Lett. (244)541-547.

Hourigan J. K., Reiners P. W., and Brandon M. T. (2005) U-Th zonation dependent alpha-ejection correction in (U-Th)/He chronometry. Geochimica et Cosmochimica Acta 69, 3349-3365.

House M. A., Wernicke B. P., Farley K. A., and Dumitru T. A. (1997) Cenozoic thermal evolution of the central Sierra Nevada, California, from (U-Th)/He thermochronometry. Earth and Planetary Science Letters 151(3-4), 167-179.

Hurford A. J. and Green P. F. (1983) The zeta age calibration of fission track dating. Isotope Geoscience 1, 285-317.

Lippolt H. J., Leitz M., Wernicke R. S., and Hagedorn B. (1994) (Uranium+thorium)/helium dating of apatite: experience with samples from different geochemical environments. Chemical Geology 112, 179-191.

McGill R., Tukey J. W., and Larsen W. A. (1978) Variations of Boxplots. The American Statistician 32, 12-16.

Min, K., Reiners, P. W., Wolff, J. A., Mundil, R. and Winters, R. L. (2005) (U-Th)/He dating of volcanic phenocrysts with high-U-Th inclusions, Jemez Volcanic Field, New Mexico. Chemical Geology (227)223-235.

Meesters A. G. C. A. and Dunai T. J. (2002a) Solving the production-diffusion equation for finite diffusion domains of various shapes Part I. Implications for low-temperature (U-Th)/He thermochronology. Chemical Geology (186)333-344.

Meesters A. G. C. A. and Dunai T. J. (2002b) Solving the production-diffusion equation for finite diffusion domains of various shapes Part II. Application to cases with α-ejection and nonhomogeneous distribution of the source. Chemical Geology (186)347-363.

Reiners P. W. (2005) Zircon (U-Th)/He Thermochronometry. In Thermochronology, Reviews in Mineralogy and Geochemistry, Vol. 58 (ed. P. W. Reiners and T. A. Ehlers), pp. 151-176.

Soderlund, P., Juez-Larre, J., Page, L.M., Dunai, T.J. (2005) Extending the time range of (U-Th)/He thermochronometry in slowly cooled terranes: Paleozoic to Cenozoic exhumation history of southeast Sweden, Earth Planet. Sci. Lett. (239)266-275.

Wolf R. A., Farley K. A., and Silver L. T. (1996) Helium diffusion and low-temperature thermochronometry of apatite. Geochimica et Cosmochimica Acta 60(21), 4231-4240.

Zingg A. (2004), Spaltspurendatierungen zur Analyse der Hebungs- und Abkühlungsgeschichte von Naxos. M.Sc. Thesis, ETH-Zürich, Switzerland.